Atmos. Chem. Phys. Discuss., 12, 13161–13199, 2012
www.atmos-chem-phys-discuss.net/12/13161/2012/
doi:10.5194/acpd-12-13161-2012

Atmospheric Chemistry and Physics Discussions

On the relationship between total ozone and atmospheric dynamics and chemistry at mid-latitudes – Part 1: Statistical models and spatial fingerprints of atmospheric dynamics and chemistry

L. Frossard[1], H. E. Rieder[2,3], M. Ribatet[1,4], J. Staehelin[2], J. A. Maeder[2], S. Di Rocco[2,5], A. C. Davison[1], and T. Peter[2]

[1]Mathematics Institute for Analysis and Applications, EPF Lausanne, Lausanne, Switzerland
[2]Institute for Atmospheric and Climate Science, ETH Zurich, Zurich, Switzerland
[3]Department of Applied Physics and Applied Mathematics, Columbia University, New York, USA
[4]Institute of Mathematics and Mathematical Modeling, University Montpellier II, Montpellier, France
[5]Department for Geography, University of Zurich, Zurich, Switzerland

Received: 30 January 2012 – Accepted: 21 April 2012 – Published: 25 May 2012

Correspondence to: L. Frossard (linda.frossard@epfl.ch) and
H. E. Rieder (hr2302@columbia.edu)

Published by Copernicus Publications on behalf of the European Geosciences Union.

ACPD
12, 13161–13199, 2012

Abstract

We use models for mean and extreme values of total column ozone on spatial scales to analyze "fingerprints" of atmospheric dynamics and chemistry on long-term ozone changes at northern and southern mid-latitudes. The *r*-largest order statistics method is used for pointwise analysis of extreme events in low and high total ozone (termed ELOs and EHOs, respectively). For the corresponding mean value analysis a pointwise autoregressive moving average model (ARMA) is used. The statistical models include important atmospheric covariates to describe the dynamical and chemical state of the atmosphere: the solar cycle, the Quasi-Biennial Oscillation (QBO), ozone depleting substances (ODS) in terms of equivalent effective stratospheric chlorine (EESC), the North Atlantic Oscillation (NAO), the Antarctic Oscillation (AAO), the El Niño/Southern Oscillation (ENSO), and aerosol load after the volcanic eruptions of El Chichón and Mt. Pinatubo. The influence of the individual covariates on mean and extreme levels in total column ozone is derived on a grid cell basis. The results show that "fingerprints", i.e., significant influence, of dynamical and chemical features are captured in both the "bulk" and the tails of the ozone distribution, respectively described by means and EHOs/ELOs. While results for the solar cycle, QBO and EESC are in good agreement with findings of earlier studies, unprecedented spatial fingerprints are retrieved for the dynamical covariates.

1 Introduction

Interest in changes in total ozone is linked to its direct influence on erythemal UV-radiation (e.g., Calbo et al., 2005), and since the detection of the Antarctic ozone hole (Farman et al., 1985) the development of the Earth's ozone layer has been a key focus in atmospheric research. The global decrease in column ozone between the 1970s and 1990s raised major concerns in the scientific community and general public. This paved the way for the "Montreal Protocol for the Protection of the Ozone Layer" (e.g., WMO,

ACPD
12, 13161–13199, 2012

1995, 2003, 2007, 2011), whose successful implementation (e.g., WMO, 2007; Mäder et al., 2010) led to a discussion on future ozone recovery and possible super-recovery expected in about 50 years (e.g., WMO, 2007, 2011; Eyring et al., 2007, 2010; SPARC CCMVal, 2010; Hegglin and Shepherd, 2009; Shepherd, 2008).

In previous studies ozone changes on spatial scales have been addressed in statistical terms by large-scale averages over latitude bands (e.g., WMO, 2003, 2007, 2011; Fioletov and Shepherd, 2005; Fioletov et al., 2002), or the application of multiple regression models (e.g., Steinbrecht et al., 2006). The former approach has difficulties, because the large-scale spatial averages usually used for analysis, such as zonal mean values, do not take spatial variability fully into account, while ozone changes vary greatly in time and space, and therefore cannot be addressed adequately by a large-scale average. Applications of multiple regression models on large spatial scales and analyses on a grid cell basis, as for satellite data sets, are rare for column ozone and the results mostly concern the influence of atmospheric dynamics and chemistry on mean column ozone, leaving the extremes unaccounted-for. Steinbrecht et al. (2006) compared multiple regression model output (for the winter season) on a global scale for observational data from TOMS and SBUV instruments with results from Chemistry-Climate Models (CCMs). Further, ozone changes have been addressed using global CCMs (e.g., Eyring et al., 2007, 2010; SPARC CCMVal, 2010; Waugh et al., 2009; Austin and Wilson, 2006). Such CCM analysis takes spatial variability into account, as ozone changes are computed on a grid cell basis due to changes in atmospheric dynamics and chemistry. Each CCM has its own parameterizations for specific processes and therefore its own strengths and deficiencies in its representation of atmospheric dynamics and chemistry. However, a lot of progress has recently been achieved in this field (e.g., Eyring et al., 2010; SPARC CCMVal, 2010).

Statistical modeling of the spatial and temporal variability of column ozone requires one to take into account the stochastic nature of physicochemical processes and their spatial and temporal variability (e.g., Chilès and Delfiner, 1999; Diggle and Ribeiro Jr., 2007). In particular there is a need for better description, modeling and forecast-

ACPD
12, 13161–13199, 2012

ing of extreme events, and an assessment of whether their distribution has changed over time, to make progress in answering important questions about the state-of-the-art treatment of ozone-climate interactions. Although geostatistics is well developed for the treatment of average values, despite recent progress (e.g., Cooley et al., 2006; Naveau et al., 2009; Ribatet et al., 2012; Padoan et al., 2010) a geostatistics of extremes that could be applied to datasets of this size is still lacking. The modeling of extremes is becoming increasingly standard as extreme value theory (EVT) develops (e.g., Coles, 2001; de Haan and Ferreira, 2006), but only a few authors have so far analyzed spatial extremes (e.g., Buishand et al., 2008; Padoan et al., 2010) and/or have dealt with massive gridded data sets (e.g., Cooley et al., 2007; Schliep et al., 2010). Although several frameworks exist for dealing with such data sets with Gaussian processes, such as approximation by Gaussian Markov fields (e.g., Rue and Held, 2005) or through composite likelihoods (e.g., Varin and Vidoni, 2005), there is much less guidance for extremes. Recently methods from EVT have been applied in total ozone research on local/regional scales (Rieder et al., 2010a, b, 2011). The present study extends these earlier analyses to large spatial data sets, using pointwise distributions for total ozone extremes. Further, the results for ozone extremes are compared with those for mean values based on a "standard" ARMA model. In both models, covariate information is included through a multiple regression term in the expression for the location parameter.

2 Data

2.1 Spatial ozone data

In this study version 2.7 of the NIWA (National Institute of Water and Atmospheric Research, New Zealand) total ozone data set is analyzed for the time period 1979–2007 for the northern (30° N–60° N) and southern (30° S–60° S) mid-latitudes. NIWA 2.7 contains daily data at a spatial resolution of 1.25° longitude by 1.0° latitude. The

ACPD
12, 13161–13199, 2012

data set is based on assimilated and homogenized data from the Total Ozone Mapping Spectrometer (TOMS), the Global Ozone Monitoring Experiment (GOME), Solar Backscatter Ultra-Violet (SBUV) retrievals and Ozone Monitoring Instrument (OMI) retrievals. Drifts between measurements of different satellite instruments have been corrected through inter-satellite instrument comparison and comparison with data from Dobson and Brewer ground-based instruments, which contribute to the Global Atmosphere Watch Program (GAW) of the World Meteorological Organization (WMO). For further details on the NIWA assimilated total ozone data set see Bodeker et al. (2005), Müller et al. (2008) and Struthers et al. (2009).

2.2 Covariates describing the state of the atmosphere, atmospheric dynamics and chemistry

Various indices describing the dynamical and chemical state of the atmosphere are used as covariates in this study, namely the 11-yr solar cycle, the Quasi-Biennial Oscillation (QBO), the El Niño/Southern Oscillation (ENSO), the North Atlantic Oscillation (NAO), the Antarctic Oscillation (AAO), ozone depleting substances (ODS) in terms of equivalent effective stratospheric chlorine (EESC) as calculated by Newman et al. (2007), and finally the stratospheric aerosol load after the major volcanic eruptions of El Chichón and Mt. Pinatubo, as given by Sato et al. (1993). Table 1 contains an overview of the data sets used (including their sources) and Fig. 1 shows the temporal evolution of the indices.

3 Methods

In this study mean and extreme values in total ozone are addressed and modeled individually on grid cell basis, to account for non-stationarity in space and time and to avoid averaging effects, e.g. caused by averaging over zonal bands.

ACPD
12, 13161–13199, 2012

We use two different models: (i) a model based on extreme value theory (EVT) to analyze extreme high (termed EHOs) and low (termed ELOs) events in total ozone (see Sect. 3.1) and (ii) an autoregressive moving average model (ARMA) for the analysis of mean values (see Sect. 3.2).

3.1 Model for total ozone extremes

This section describes the role of the r-largest order statistics model in extreme value theory (e.g., Coles, 2001; de Haan and Ferreira, 2006) and gives details on its implementation in our context. The modeling of extreme events covers both very high (maxima) and very low (minima) events but the equality

$$\min_{i=1,\ldots,n}(Y_i) = -\max_{i=1,\ldots,n}(-Y_i)$$

shows that it suffices to define models for maxima, on which we focus hereafter.

There are several methods for modeling extremes of univariate time series. In the block maxima model, the data are grouped into blocks of specific length given by a time period (e.g., a year or a month) and the sequence of block maxima is modeled as an independent sample from the Generalized Extreme Value (GEV) distribution. To avoid the waste of data resulting from retaining only one observation per block, all exceedances of a threshold can be modeled using the Generalized Pareto Distribution (GPD) (Pickands, 1975; Davison and Smith, 1990). The r-largest order statistics model (Coles, 2001), which we use below, can be seen as a compromise between the block maxima and peaks over threshold methods, as the data are split into blocks, but the $r \geq 1$ largest observations per block are used.

The selection of the threshold, or equivalently the value of the block length r, is crucial, because it determines the quality of the model through a trade-off between bias and variance. There are graphical methods for threshold selection but they require individual inspection. Rieder et al. (2010b, 2011) used these methods in their application of the GPD model for threshold exceedances to total ozone data on local scale. For the

ACPD
12, 13161–13199, 2012

thousands of time series in the NIWA assimilated total ozone data set, however, a form of automatic threshold selection is provided by the *r*-largest order statistics model, or equivalently by taking as threshold the empirical quantile at a fixed level (e.g., 95 %).

The size of the NIWA data set (the mid-latitudes as defined here contain 8640 grid cells for each hemisphere) imposes practical constraints on the general modeling approach. Since the NIWA data cover the whole globe, a spatial model for extremes would be natural. One possibility is max-stable processes (de Haan, 1984; Schlather, 2002) but current fitting methods for them (Padoan et al., 2010; Gholamrezaee, 2010) are computationally infeasible for massive (gridded) data sets. Therefore we fit the *r*-largest order statistics model separately to each grid cell, as if the neighboring cells did not exist, using methods for univariate extremes. This pointwise approach allows us to assess how spatial variation of the model parameters affects the grid cell extremes (which is of major interest for the study), but it does not allow us to model the joint behavior of extremes. This is a topic of continuing research.

Total ozone data at mid-latitudes show strong non-stationarity, owing to the seasonality of atmospheric chemistry and dynamics. This must be accounted for in the model, and particularly in the threshold selection. In the model non-stationarity is included by letting the location parameter depend on time-dependent covariates (see below). Furthermore, we choose the blocks to be months, giving an individual threshold for each year-month-combination, and allowing also for non-stationarity effects other than seasonality.

Maximum likelihood estimation of the *r*-largest order statistics model can be done more or less automatically and with reasonable computational effort even for large regions, as there exists a closed-form likelihood and threshold selection is automatic once *r* is fixed. A weakness of this procedure is that the days of occurrence of the extreme events are not taken into account, implying that clusters of extremes are not recognized as such, neither in the middle of the month nor at the transition between two months. To avoid this, declustering of the extreme events of each time series would be needed, but the required effort for declustering both maxima and minima of 8640

ACPD
12, 13161–13199, 2012

time series for each hemisphere was considered to be disproportionate to the scope of this study. In practice declustering typically has little effect on parameter estimates, though by reducing the sample size it does affect their precision.

The log likelihood of the r-largest order statistics model, which is derived from the Poisson point process model for extremes (Coles, 2001; de Haan and Ferreira, 2006), is for each block $k = 1, \ldots, b$

$$\ell_k(\mu,\sigma,\xi) = -r\log\sigma - \left(1+\xi\frac{y_k^{(r)}-\mu}{\sigma}\right)_+^{-1/\xi} - \left(1+\frac{1}{\xi}\right)\sum_{j=1}^{r}\log\left(1+\xi\frac{y_k^{(j)}-\mu}{\sigma}\right)_+, \quad (1)$$

where the location parameter μ and shape parameter $\xi \in \mathbb{R}$, the scale parameter $\sigma > 0$, $x_+ = \max(x,0)$ and $y_k^{(1)} \geq \cdots \geq y_k^{(r)}$ are the r largest observations in block k. The assumed independence of the blocks implies that the log likelihood for the whole data is the sum of the block contributions given in Eq. (1).

The asymptotic normality of the maximum likelihood estimator, which should be applicable to our estimates based on $b = 348$ months of data, allows us to test whether the parameter estimates are significant by a z-test. Under the null hypothesis that the estimate is zero, the estimate divided by its standard error has an approximate standard normal distribution, so the p-value is easily determined.

Next we describe the explicit structure of the implemented model(s) by treating threshold selection and the modeling of non-stationarity.

Let $\mathcal{X}$ be the set of analyzed grid cells and let GEV_r denote the r-largest order statistics model. The observed ozone extremes $y(x,t)$ at a fixed cell $x \in \mathcal{X}$ and month t are modeled as

$$y(x,t) \sim \mathrm{GEV}_r\Big(\mu(x,t),\, \sigma(x),\, \xi(x)\Big),$$

where the non-stationary location parameter μ takes a linear form

$$\mu(x,t) = \mathbf{Z}(t)\boldsymbol{\beta}(x), \quad (2)$$

ACPD
12, 13161–13199, 2012

in which $\mathbf{Z}(t)$ is one row of the design matrix $\mathbf{Z}(\boldsymbol{t})$, $\boldsymbol{t}$ being the vector of observation times. The design matrix $\mathbf{Z}(\boldsymbol{t})$ is composed of seasonality terms and covariates describing chemical and dynamical processes in the atmosphere (see below). All covariates are taken at a monthly resolution, so the same covariate value is used for the r observations of each month. Even though the atmospheric covariates vary across space, a "global" design matrix was used for all grid cells, so that the resulting maps of parameter estimates $\{\beta(x) : x \in \mathcal{X}\}$, where β is one component of the coefficient vector $\boldsymbol{\beta}$, are interpretable and comparable.

To be consistent with the structure of Eq. (2), the set of covariates must be the same for all grid cells in one hemisphere. Since fitting the model to the complete grid requires much computation time, it is infeasible to fit many different models for each grid cell. Instead we identified the most promising set of covariates on a subset of 72 grid points, using standard model selection techniques. After extensive exploratory analysis, the best model was found to be

$$\begin{aligned}\mu(x,t) = &\beta_0 + \sum_{i=1}^{3}\left(\beta_{2i-1}\cos\frac{2\pi t}{\phi_i} + \beta_{2i}\sin\frac{2\pi t}{\phi_i}\right) + \beta_7\mathrm{EESC}(t) + \beta_8\mathrm{SOLAR}(t) \\ &+ \beta_9\mathrm{QBO}_{30}(t) + \beta_{10}\mathrm{QBO}_{50}(t) + \beta_{11}\mathrm{ENSO}(t) + \beta_{12}\left\{\begin{matrix}\mathrm{AAO}(t)\\ \mathrm{NAO}(t)\end{matrix}\right\} \\ &+ \beta_{13}\mathrm{CHICHON}(t) + \beta_{14}\mathrm{PINATUBO}(t),\end{aligned} \tag{3}$$

where ϕ_i are the frequencies allowing for 1-yr, 6-month and 4-month seasonalities, i.e., $(\phi_1, \phi_2, \phi_3) = (12, 6, 4)$, and the coefficients $\beta_0, \ldots, \beta_{14}$ depend on grid cell $x \in \mathcal{X}$. The other covariates in Eq. (3) are listed in Sect. 2.2. The AAO and NAO are only used for the Southern and the Northern Hemisphere, respectively; and the covariates for the volcanic eruptions of El Chichón and Mt. Pinatubo are extracted from the SATO-Index for the corresponding hemisphere (see Fig. 1). A detailed description of these covariates and their potential interaction with the ozone levels is given in Sect. 4.

ACPD
12, 13161–13199, 2012

The model with location parameter μ given in Eq. (3), where the regression parameters $\beta_0, \ldots, \beta_{14}$ do not depend on time t, will be referred to as the *annual model* because there is only one coefficient for each covariate, expressing its effect over the whole year. Since the influence of the covariates is likely to vary across the seasons, we fitted a second *seasonal model* in which some covariates are split into four pieces, one for each season defined by December-January-February, March-April-May, June-July-August and September-October-November. For instance the term $\beta_7 \mathrm{EESC}(t)$ in Eq. (3) can be replaced by

$$\beta_{7,\mathrm{Spring}}\mathrm{EESC}_{\mathrm{Spring}}(t) + \beta_{7,\mathrm{Summer}}\mathrm{EESC}_{\mathrm{Summer}}(t) + \beta_{7,\mathrm{Autumn}}\mathrm{EESC}_{\mathrm{Autumn}}(t) + \beta_{7,\mathrm{Winter}}\mathrm{EESC}_{\mathrm{Winter}}(t)$$

where $\mathrm{EESC}_{\lozenge}$ equals the EESC values for the months of season $\lozenge$ and zero for the other months. In this study EESC, SOLAR, QBO_{30} and QBO_{50}, ENSO and AAO/NAO were split into seasonal components. In the seasonal model, the regression coefficients $\beta_7, \ldots, \beta_{12}$ are thus time-dependent through a periodic step function. The annual model may be nested into the seasonal one by setting $\beta_{\cdot,\mathrm{Spring}} = \beta_{\cdot,\mathrm{Summer}} = \beta_{\cdot,\mathrm{Autumn}} = \beta_{\cdot,\mathrm{Winter}}$, so likelihood ratio tests allow one to assess whether these covariates have a varying impact over the year (see Sect. 4.1).

As for the selection of r, which is the threshold selection for the r-largest order statistics model, we reasoned as follows: considering that a month has about 30 days, r should not exceed 3 for the observations to be "extreme", as the resulting threshold corresponds roughly to the empirical 90 %-quantile. In view of the general uncertainty that might govern the estimation due to the high number of covariates, we chose $r = 3$ to increase the precision of the estimates. For the purpose of bias inspection, models with $r = 1$ and $r = 2$ were also fitted. They showed the same patterns, but as anticipated, there were larger standard errors and hence less significant p-values.

ACPD
12, 13161–13199, 2012

3.2 ARMA model for total ozone mean values

The multiple linear regression model, a standard tool for modeling and analyzing changes in a variable of interest (e.g., total ozone) and the contribution of individual covariates to these changes, is widely used in atmospheric science. In a first step we therefore also used multiple linear regression models for the analysis of monthly total ozone mean values at both northern and southern mid-latitudes (on grid cell basis, in analogy to the model for extreme events). However, the residuals of this model were significantly correlated, showing that the assumption of independent errors in the linear regression model does not hold for our data.

We therefore keep the linear regression term $\mathbf{Z}(t)\boldsymbol{\beta}(x)$ to express non-stationarity and model the errors by the classic model for stationary time series, the autoregressive moving average (ARMA) process (e.g., Brockwell and Davis, 1996). A stationary time series $\{Y_t\}$ is an ARMA process of order (p,q) if it can be written as

$$Y_t = \sum_{i=1}^{p} \phi_i Y_{t-i} + \varepsilon_t + \sum_{j=1}^{q} \theta_j \varepsilon_{t-j}, \tag{4}$$

where $\{\varepsilon_t\}$ is white noise.

If $y(x,t)$ denotes the monthly mean value at cell $x \in \mathcal{X}$ and month t of the NIWA data set, it is modeled as

$$y(x,t) = \mathbf{Z}(t)\boldsymbol{\beta}(x) + \eta(x,t), \tag{5}$$

where

$$\eta(x,t) = \phi\, \eta(x,t-1) + \varepsilon(x,t) + \theta\, \varepsilon(x,t-1), \tag{6}$$

and $\varepsilon(x,t) \overset{\text{ind}}{\sim} N\left(0, \sigma(x)^2\right)$ is Gaussian white noise.

The design matrix $\mathbf{Z}(t)$ is identical with that used in the extremes model (see above), comprising seasonality terms and covariates that describe atmospheric dynamics and

ACPD
12, 13161–13199, 2012

chemistry at a monthly resolution. The term $\mathbf{Z}(t)\boldsymbol{\beta}(x)$ in Eq. (5) thus equals the right hand side of Eq. (3).

As in the extremes model (see Sect. 3.1) we fitted two ARMA models with different regression terms, an annual model, where the individual covariates do not depend on time and only one coefficient is used for each covariate, and a seasonal model, where some of the covariates are split into four seasons (see above) and depend thus on time through a periodic step function.

Since the fitting of an ARMA model is much faster than for the r-largest order statistics model, we fitted several ARMA models with different orders (p, q) and compared their AIC (Akaike Information Criterion). There is no uniformly best model over all grid cells but in all cases (north, south, annual, seasonal) the ARMA(1,1) model performs quite well in a majority of grid cells, so that we chose this model (see the expression for η in Eq. 6).

4 Results

Inference about the effect of a single covariate based on pointwise modeling of the grid cells may be performed by testing for each grid cell the hypothesis that the covariate has no effect, but interpreting the results is not straightforward, because of the large number of tests that must be performed, based on highly correlated data. If the same false positive rate α were used for every cell, and if all the null hypotheses were true, then we would expect a proportion α of them to be falsely rejected. Thus with 8640 cells and with $\alpha = 0.05$, we would expect to incorrectly find a significant effect of the covariate at 432 cells, and these will tend to be grouped owing to spatial correlation. Ventura et al. (2004) discuss approaches to multiple testing that control the false discovery rate (FDR), i.e., the expected proportion of falsely rejected null hypotheses among the total rejected null hypotheses. Using the FDR is attractive because in practice the number of rejected null hypotheses is known but the number of true null hypotheses is not. The basic FDR approach assumes independence of the p-values, but Ventura et al. (2004)

ACPD
12, 13161–13199, 2012

suggest that it can also be used for data with light spatial correlation. Unfortunately, and as would be anticipated, the NIWA data show very strong correlations, and this undermines the case for using the basic FDR approach. Another method often used in climate science, the field significance method (Livezey and Chen, 1983), seems inappropriate in the setting of extremes. The topic of multiple testing is undergoing rapid development and a definitive treatment in the present context cannot yet be provided, so in order to assess the strength of the conclusions below, we applied four approaches to the z-statistics for the covariate effects on extremes: making no correction for multiple testing, FDR, a conservative version of FDR that allows for general correlation in the z-statistics, and the ultra-conservative Bonferroni correction. We also used various scenarios with inflated standard errors to account for potential temporal correlation in the extremes. We comment briefly on the results of this sensitivity analysis when discussing the specific effects below, and in the companion paper to this article.

4.1 Evaluation of the statistical models

First, we show results on the evaluation of the model(s) described above. Gridpointwise likelihood ratio tests between the annual model (null hypothesis H_0) and seasonal model (alternative hypothesis H_1), showed that the use of the more complicated seasonal model is justified for both the EVT and the ARMA model (see Table 2 for a complete summary). For the r-largest order statistics model the proportions of grid cells where H_0 is rejected at the 5 %-level lie far above 80 % for both hemispheres and types of extremes, whereas they are much lower but still above 50 % for the ARMA model fitted to the means. This reduction in the proportion of rejections is probably due to the better incorporation of correlation between the observations in the ARMA model than in the r-largest order statistics model, where the blocks are assumed to be independent. Hence the proportions obtained for the EVT models are likely to be too high.

As the comparison of fitted values or residuals with observations depends on time, model evaluation on the complete grid is intractable. Therefore Fig. 2 provides diag-

ACPD
12, 13161–13199, 2012

nostic plots for two representative grid cells, using the seasonal model for EHOs, and Fig. 3 provides an example for the seasonal model for mean values. Overall the fit seems reasonable, despite a small bias in the residuals of the EVT model (Fig. 2c and f); this only affects the intercept of our model, and not the regression coefficients of the covariates. A comparison with the same model for $r = 1$ showed that estimates of the covariate coefficients from the two models are consistent, and diagnostic plots of the model with $r = 1$ show a good fit and no bias, indicating no fundamental trouble with the model when $r > 1$. Simulations suggest that the bias stems from temporal correlation of the underlying time series.

4.2 Spatial patterns

The spatial models allow to analyze the influence of the individual covariates (see Fig. 1 and Sect. 2.1) on (i) EHOs, (ii) ELOs and (iii) mean values. For analytical and illustrative reasons it is convenient to plot pointwise regression coefficient estimates for the covariates, their related standard errors and the p-values of the z-test in the context of maximum likelihood estimation on a grid cell basis; although our analysis provides additional information about the pointwise distribution of ozone extremes, such information is beyond the scope of the present study. The test values (p-values) are especially useful when assessing the significance of a covariate at a grid cell. We consider a covariate to be significant whenever the corresponding p-value is less than 1 %, bearing in mind that the calculated p-values are probably rather too small, owing to the effects of temporal correlation in the extremes.

Below we focus on spatial patterns in the three "standard" covariates included in analyses of long-term ozone changes (e.g., in the WMO/UNEP Ozone Assessment Reports: WMO, 2003, 2007, 2011), i.e., the solar cycle, QBO and EESC, and on additional frequently used dynamical covariates, namely the NAO and AAO indices. A companion paper (Rieder et al., 2012, from here on referred to as Part 2) gives a detailed discussion on the spatial fingerprints of the volcanic eruptions of El Chichón and Mt. Pinatubo and of the fingerprints of the El Niño/Southern Oscillation, on which scientific interest

ACPD
12, 13161–13199, 2012

has recently focused. Part 2 also reports on the contribution of the individual covariates to long-term total ozone changes for selected regions of interest at northern and southern mid-latitudes.

4.2.1 Solar cycle

Solar variability described by the 11-yr solar cycle (describing changes in solar irradiance through changes in sunspot number) (see Fig. 1a) influences stratospheric ozone as UV-radiation varies with an amplitude of 6–8 % between solar maxima and minima (e.g., Chandra and McPeters, 1994). Previous studies found that at mid-latitudes about 2 % of total ozone variability can be explained through changes in the solar cycle. However, long-term trends in column ozone of the last decades cannot be explained by solar variability (e.g., Harris et al., 2008; Chandra and McPeters, 1994).

The *p*-values show that the solar cycle seems to be significant on an annual basis for much of the northern and southern mid-latitudes (see Fig. 4), which is in general agreement with earlier studies (e.g., Steinbrecht et al., 2006). However, two things are important to note: (i) the area showing highly significant influence of the solar cycle is much larger for extremes than mean values and (ii) on a seasonal basis, high variability is found in the spatial extent of the significance area (not shown here), as during spring and winter significant influence of the solar cycle is restricted towards lower latitudes, in agreement with the strong influence of the solar cycle on ozone production in the tropical region. Sensitivity analysis shows that the effect persists when any of the corrections for multiple testing are applied, though as expected the region of significance becomes smaller.

4.2.2 Quasi-Biennial Oscillation (QBO)

The QBO dominates the variability of the equatorial stratosphere. Seen as a composite of equatorial zonal winds, it shows faster and more regular downward propagation during the westerly phase and stronger intensity and longer duration during

ACPD
12, 13161–13199, 2012

the easterly phase. The mean period of the QBO is about 28 months. Maxima in the variability are larger during the westerly than the easterly phase and are found close to the descending easterly and westerly shear zones (e.g., Baldwin et al., 2001). Although the QBO is a tropical phenomenon, it affects stratospheric flow from pole to pole due to modulation of the effects of extra-tropical waves. Connection between the QBO and the extra-tropical atmosphere (e.g., mid-latitudes) must be seen in the context of the seasonal cycle and variability of the extra-tropical stratosphere. During winter, the high-latitude stratosphere cools and a deep westerly polar vortex is formed. During spring and summer, the vortex diminishes and the westerlies are replaced by easterlies due to increased solar heating. As the Northern Hemisphere has much greater land-mass than the Southern Hemisphere, tropospheric waves have larger amplitudes in the Northern Hemisphere. Therefore, the northern hemispheric winter stratosphere is much more disturbed than its southern counterpart. Consequently the northern polar vortex can already be disrupted by large-scale planetary waves in mid-winter, when the exchange of westerlies with easterlies in high latitudes causes strong sudden stratospheric warming events (e.g., Waugh and Randel, 1999). Further, various studies have also described an influence of the QBO on other constituents of the atmosphere, such as methane and water vapor (e.g., Baldwin et al., 2001).

In this study the QBO at two different pressure levels (30 and 50 hPa, with no lag) (see Fig. 1b, c) was used as covariate in the spatial models. The *p*-values in Fig. 5 and 6 show that QBO at both pressure levels seems to be significant over large areas of the northern and southern mid-latitudes. Coefficient estimates for both QBO_{30} and QBO_{50} are highly significant towards the equatorial regions of the northern and southern mid-latitudes. At northern mid-latitudes the coefficient estimates for QBO_{30} show a smooth staggered gradient towards high latitudes, while the coefficient estimates for QBO_{50} show a band-like structure where significant regions towards low and high latitudes are split by an insignificant band. While coefficient estimates are positive for lower latitudes, they turn negative after the transition zone towards polar latitudes. This structure is possibly related to a connection between the QBO and the Brewer-Dobson circulation,

ACPD
12, 13161–13199, 2012

as Haklander et al. (2006) showed that the mean zonal wind pattern can alter the wave driving of the Brewer-Dobson circulation. This second significance region towards northern polar regions, identified in our analysis, is in good agreement with earlier work discussing the influence of the QBO on column ozone at high latitudes (e.g., Oltmans and London, 1982; Garcia and Solomon, 1987; Lait et al., 1989; Randel and Cobb, 1994; Baldwin et al., 2001). The effects of QBO_{30} are more important than those of QBO_{50}, with the latter becoming much less striking under sensitivity analysis.

4.2.3 Ozone depleting substances (ODS)

Anthropogenic emissions of ODS (ozone depleting substances such as chlorofluorocarbons) increased from the early 1950s until the late 1980s, when the Montreal Protocol was signed. The scale of EESC (equivalent effective stratospheric chlorine) describes the effect of stratospheric ozone depletion caused by anthropogenic emissions of ODS in an integral way (note that we use the EESC scale for mid-latitudes here). EESC peaked in the second half of the 1990s (the transport of EESC from the release of ODS near surface into the stratosphere causes a shift between maximal emissions of ODS and EESC) (see Fig. 1i). Chemical ozone depletion is particularly large during the winter and spring seasons when ozone destruction occurs inside the polar vortex, caused by heterogeneous chemical reactions taking place on polar stratospheric clouds (e.g., Peter, 1997; Solomon, 1999). Apart from the atmospheric burden in ODS, stratospheric temperature is the main driver of ozone loss within the polar vortex (e.g., Rex et al., 2004).

At northern mid-latitudes the relation between EESC and column ozone is negative and significant in almost all areas (see Fig. 7) (except in a region north to 50° N and around 120° W where EESC is barely significant, probably because dynamic variability disturbs the relation between column ozone and EESC). In our sensitivity analysis, EESC remains the strongest covariate under any multiple testing corrections. Coefficient estimates in Fig. 7 for both extremes and mean values show a gradient increasing towards high latitudes. At southern mid-latitudes, the influence of ODS shows as

ACPD
12, 13161–13199, 2012

a “stable staggered” gradient in coefficient estimates which may result from the less disturbed atmospheric flow due to reduced land-mass.

4.2.4 North Atlantic Oscillation (NAO)

Inter-annual and decadal changes in Northern Hemisphere tropospheric meteorology and stratospheric dynamics are strongly related to the variability in the North Atlantic (NAO) and the Arctic Oscillation (AO). Several studies have shown that the NAO affects changes in the direction and intensity of the dominant westerly tropospheric jet stream (e.g., Orsolini and Limpasuvan, 2001) and thereby influences European winter/spring climate and the strength of the Arctic polar vortex affecting the stratospheric ozone layer (e.g., Appenzeller et al., 2000; Thompson and Wallace, 2000; Orsolini and Limpasuvan, 2001; Hadjinicolaou et al., 2002; Orsolini and Doblas-Reyes, 2003). Here we use a NAO index, following Hurrel (2009), built by the principal components of the leading empirically-determined orthogonal function of seasonal sea level pressure anomalies over the Atlantic sector (defined as: 20° N–80° N, 90° W–40° E).

The coefficient estimates for the NAO, in winter and spring (see Fig. 8), are found to be significant for much of the northern mid-latitudes, and this significance varies but persists with any of the multiple testing corrections. Largest positive coefficients are found over Labrador/Greenland, the North Atlantic sector and over the Norwegian Sea, while largest negative coefficient estimates are found over Europe, Russia and the Eastern United States. While regions with positive coefficient estimates will show increased column ozone during positive phases of the NAO and decreased column ozone during its negative phases, the converse is true for regions with negative coefficient estimates (see also contribution to long-term ozone changes at different regions presented in Part 2 of this paper). This relation between column ozone and the mode of the NAO can be explained by pressure gradients, which are increased during positive phases of the NAO due to a deeper than usual Icelandic low and a stronger than usual sub-tropical high pressure system. This increased pressure gradient results in more and stronger winter storms crossing the Atlantic and a shift of storm tracks towards

ACPD
12, 13161–13199, 2012

the north. During the negative phase of the NAO the converse occurs, i.e., a weaker sub-tropical high and Icelandic low lead to a reduced pressure gradient, and therefore to fewer and weaker winter storms on a more west-east pathway. Compared to other covariates discussed, the NAO "fingerprint" is of similar spatial extent for both extremes and mean values, but the magnitude of influence on total ozone is larger for EHOs and ELOs than for mean values, confirming the importance of atmospheric dynamics for total ozone variability and changes (see Part 2 and Rieder et al., 2010a, b, 2011).

4.2.5 Antarctic Oscillation (AAO)

The semi-annual oscillation (SAO) at mid- and high latitudes in the Southern Hemisphere is related to the depth of the troposphere and to the weakening and expansion of the circumpolar trough of low pressure surrounding Antarctica from March–June and September–December (e.g., van Loon, 1967, 1972; Hurrell, 2009).

During the high phase of the Antarctic Oscillation (AAO), the Lagrangian mean circulation, responsible for the transport of ozone from the tropics to the polar region, is strongly reduced. Wave refraction triggers this process: during the high phase, the polar vortex refracts more wave activity in the tropics and breaking of these waves strengthens the vortex due to the inside transport of momentum (e.g., Thompson and Wallace, 2000). During the low phase of the AAO the opposite occurs: a weaker vortex decelerates more when waves are defracting in.

As for the NAO in the Northern Hemisphere, the contribution of the AAO to extremes and mean values seems to be highly significant over large parts of the southern mid-latitudes (see Fig. 9). Results of the sensitivity analysis for the AAO are similar to those for the NAO, confirming presence of the effects with any of the multiple testing corrections. Interestingly the central southern mid-latitudes show especially highly significant (negative) coefficient estimates for the AAO. This may be related to enhanced wave activity in the tropics (see also Schnadt Poberaj et al., 2011), leading to enhanced ozone transport from the tropics to the extra-tropics (compare also with results for ENSO shown in Part 2) and a strengthening of the southern ozone "collar". The AAO was

ACPD
12, 13161–13199, 2012

found to have also significant influence on the dynamical masking of the Mt. Pinatubo eruption at southern mid-latitudes, which is discussed in detail in Part 2.

5 Discussion and conclusion

In this study statistical models, including important covariates describing the state of the atmosphere (solar cycle, QBO, ENSO, NAO, AAO, ODS and volcanic eruptions), have been used to analyze changes in extreme (EHOs and ELOs using the *r*-largest order statistics model) and mean values (using an ARMA model) of total ozone at northern and southern mid-latitudes. The results show that "fingerprints" of dynamical and chemical features are captured in both the "bulk" and the tails of the distribution of total ozone time series. However, "fingerprints" of atmospheric dynamics (NAO, AAO) are better represented in the extremes and can be partly overlooked in a mean value context. This confirms results of earlier local/regional studies (Rieder et al., 2010a, 2011).

For the three "standard" covariates solar cycle, QBO and EESC, significant influence was found almost throughout the northern and southern mid-latitudes, in good agreement with previous studies (e.g., Steinbrecht et al., 2006; WMO, 2003, 2007, 2011). However, there are several important features to note: (i) regarding the "fingerprints" of the solar cycle, the area highly significantly influenced is much larger for extremes than for mean values and there is high seasonal variability (not shown here). (ii) For the QBO at both pressure levels analyzed (30 and 50 hPa) large significant areas are found at both northern and southern mid-latitudes, especially towards equatorial regions. An interesting feature is the band-like structure found for QBO_{50}: an insignificant band at central mid-latitudes splits two highly significant areas towards equatorial and polar regions. This structure might be related to a connection between the QBO and the Brewer Dobson circulation at this pressure level, where zonal winds can alter wave driving (e.g., Haklander et al., 2006). (iii) Regarding the influence of ozone depleting substances, the results for the EESC-covariate establish the strong influence of

ACPD
12, 13161–13199, 2012

ODS on ozone throughout mid-latitudes. At northern mid-latitudes a gradient is found in EESC-coefficients, increasing towards high latitudes, which can be interpreted as resulting from the interaction between ozone production in the tropics, ozone transport to mid- and high-latitudes (due to the Brewer-Dobson circulation) and enhanced ozone depletion in polar regions (especially during winter and early spring). This pattern is less pronounced (but still preserved) at southern mid-latitudes, most likely due to the reduced land-mass leading to less disturbed atmospheric flow.

For the North Atlantic Oscillation, strong influence on column ozone is found over Labrador/Greenland, the Eastern United States, the Euro-Atlantic sector and Central Europe. For the NAO's southern counterpart, the AAO, strong influence on column ozone is found at lower southern mid-latitudes, including the southern parts of South America and the Antarctic Peninsula, and central southern mid-latitudes. At central southern mid-latitudes highly significant negative coefficient estimates found for the AAO can probably be related to enhanced wave activity in the tropics leading to enhanced ozone transport from the tropics to the extra-tropics. Results for both NAO and AAO confirm the importance of atmospheric dynamics for ozone variability and changes from local/regional to global scale.

Finally, we refer to the companion paper (Rieder et al., 2012) for the spatial analysis of fingerprints of the volcanic eruptions of El Chichón and Mt. Pinatubo and the El Niño/Southern Oscillation. There we discuss the important role of dynamical covariates (AAO and ENSO) on amplifying/weakening the effect of volcanic eruptions at southern mid-latitudes and provide a detailed overview of the contribution of the individual covariates to long-term total ozone changes (1979–2007), in the mean and extreme values, for various regions of interest.

Acknowledgements. H. E. R., L. F., M. R., J. S., and A. C. D. acknowledge funding by the Competence Centre for the Environment and Sustainability (CCES) within the ETH-domain in Switzerland within the project EXTREMES: "Spatial extremes and environmental sustainability: statistical methods and applications in geophysics and the environment". H. E. R. acknowledges also funding of the Swiss National Science Foundation through the Fellowship Grant PBEZP2-134426.

ACPD
12, 13161–13199, 2012

The authors are grateful to the New Zealand National Institute of Water and Atmospheric Research (NIWA) for providing the data of the NIWA assimilated total ozone data set.

The Software R (R Development Core Team, http://www.R-project.org) was used for the statistical analysis.

References

Appenzeller, C., Weiss, A. K., and Staehelin, J.: North Atlantic oscillation modulates total ozone winter trends, Geophys. Res. Lett., 27, 1131–1134, 2000.

Austin, J. and Wilson, R. J.: Ensemble simulations of the decline and recovery of stratospheric ozone, J. Geophys. Res.-Atmos., 111, D16314, doi:10.1029/2005jd006907, 2006.

Baldwin, M. P., Gray, L. J., Dunkerton, T. J., Hamilton, K., Haynes, P. H., Randel, W. J., Holton, J. R., Alexander, M. J., Hirota, I., Horinouchi, T., Jones, D. B. A., Kinnersley, J. S., Marquardt, C., Sato, K., and Takahashi, M.: The quasi-biennial oscillation, Rev. Geophys., 39, 179–229, 2001.

Bodeker, G. E., Shiona, H., and Eskes, H.: Indicators of Antarctic ozone depletion, Atmos. Chem. Phys., 5, 2603–2615, doi:10.5194/acp-5-2603-2005, 2005.

Brockwell, P. J. and Davis, R. A.: Introduction to Time Series and Forecasting, Springer, New York, 1996.

Buishand, T. A., de Haan, L., and Zhou, C.: On spatial extremes: with application to a rainfall problem, Ann. Appl. Stat., 2, 624–642, 2008.

Calbo, J., Pages, D., and Gonzalez, J. A.: Empirical studies of cloud effects on UV radiation: a review, Rev. Geophys., 43, RG2002, doi:10.1029/2004rg000155, 2005.

Chandra, S. and McPeters, R. D.: The solar-cycle variation of ozone in the stratosphere inferred from NIMBUS-7 and NOAA-11 satellites, J. Geophys. Res.-Atmos., 99, 20665–20671, 1994.

Chilès, J. P. and Delfiner, P.: Geostatistics: Modelling Spatial Uncertainty, Wiley, New York, 1999.

Coles, S.: An Introduction to Statistical Modeling of Extreme Values, Springer Series in Statistics, Springer, London, 2001.

Cooley, D., Naveau, P., and Poncet, P.: An Introduction to Statistical Modelling of Extreme Values, Springer Lecture Notes in Statistics Edition, Springer, New York, 2006.

ACPD

12, 13161–13199, 2012

Cooley, D., Nychka, D., and Naveau, P.: Bayesian spatial modeling of extreme precipitation return levels, J. Am. Stat. Assoc., 102, 824–840, doi:10.1198/016214506000000780, 2007.
Davison, A. C. and Smith, R. L.: Models for exceedances over high thresholds (with discussion), J. Roy. Stat. Soc. B, 52, 393–442, 1990.
Diggle, P. J. and Ribeiro Jr., P. J.: Model-Based Geostatistics, Springer Series in Statistics, Springer, New York, USA, 2007.
Eyring, V., Waugh, D. W., Bodeker, G. E., Cordero, E., Akiyoshi, H., Austin, J., Beagley, S. R., Boville, B. A., Braesicke, P., Bruhl, C., Butchart, N., Chipperfield, M. P., Dameris, M., Deckert, R., Deushi, M., Frith, S. M., Garcia, R. R., Gettelman, A., Giorgetta, M. A., Kinnison, D. E., Mancini, E., Manzini, E., Marsh, D. R., Marches, S., Nagashima, T., Newman, P. A., Nielsen, J. E., Pawson, S., Pitari, G., Plummer, D. A., Rozanov, E., Schraner, M., Scinocca, J. F., Semeniuk, K., Shepherd, T. G., Shibata, K., Steil, B., Stolarski, R. S., Tian, W., and Yoshiki, M.: Multimodel projections of stratospheric ozone in the 21st century, J. Geophys. Res., 112, D16303, doi:10.1029/2006JD008332, 2007.
Eyring, V., Cionni, I., Bodeker, G. E., Charlton-Perez, A. J., Kinnison, D. E., Scinocca, J. F., Waugh, D. W., Akiyoshi, H., Bekki, S., Chipperfield, M. P., Dameris, M., Dhomse, S., Frith, S. M., Garny, H., Gettelman, A., Kubin, A., Langematz, U., Mancini, E., Marchand, M., Nakamura, T., Oman, L. D., Pawson, S., Pitari, G., Plummer, D. A., Rozanov, E., Shepherd, T. G., Shibata, K., Tian, W., Braesicke, P., Hardiman, S. C., Lamarque, J. F., Morgenstern, O., Pyle, J. A., Smale, D., and Yamashita, Y.: Multi-model assessment of stratospheric ozone return dates and ozone recovery in CCMVal-2 models, Atmos. Chem. Phys. Discuss., 10, 11659–11710, doi:10.5194/acpd-10-11659-2010, 2010.
Farman, J. C., Gardiner, B. G., and Shanklin, J. D.: Large losses of total ozone in Antarctica reveal seasonal ClO_x/NO_x interaction, Nature, 315, 207–210, 1985.
Fioletov, V. E. and Shepherd, T. G.: Summertime total ozone variations over middle and polar latitudes, Geophys. Res. Lett., 32, L04807, doi:10.1029/2004gl022080, 2005.
Fioletov, V. E., Bodeker, G. E., Miller, A. J., McPeters, R. D., and Stolarski, R.: Global and zonal total ozone variations estimated from ground-based and satellite measurements: 1964–2000, J. Geophys. Res.-Atmos., 107, 4647, doi:10.1029/2001jd001350, 2002.
Garcia, R. R. and Solomon, S.: A possible relationship between interannual variability in Antarctic ozone and the Quasi-Biennial Oscillation, Geophys. Res. Lett., 14, 848–851, 1987.
Gholamrezaee, M. M.: Geostatistics of extremes: a composite likelihood approach, PhD thesis, École Polytechnique Federale de Lausanne (EPFL), Lausanne, 2010.

ACPD
12, 13161–13199, 2012

de Haan, L.: A spectral representation of max-stable processes, Ann. Probab., 12, 1194–1204, 1984.
de Haan, L. and Ferreira, A.: Extreme Value Theory: An Introduction, Springer Series in Operations Research and Financial Engineering, Springer, New York, USA, 2006.
Hadjinicolaou, P., Jrrar, A., Pyle, J. A., and Bishop, L.: The dynamically driven long-term trend in stratospheric ozone over northern middle latitudes, Q. J. Roy. Meteorol. Soc., 128, 1393–1412, 2002.
Haklander, A. J., Siegmund, P. C., and Kelder, H. M.: Analysis of the frequency-dependent response to wave forcing in the extratropics, Atmos. Chem. Phys., 6, 4477–4481, doi:10.5194/acp-6-4477-2006, 2006.
Harris, N. R. P., Rex, M., Goutail, F., Knudsen, B. M., Manney, G. L., Muller, R., and von der Gathen, P.: Comparison of empirically derived ozone losses in the Arctic vortex, J. Geophys. Res.-Atmos., 107, 8264, doi:10.1029/2001jd000482, 2002.
Harris, N. R. P., Kyrö, E., Staehelin, J., Brunner, D., Andersen, S.-B., Godin-Beekmann, S., Dhomse, S., Hadjinicolaou, P., Hansen, G., Isaksen, I., Jrrar, A., Karpetchko, A., Kivi, R., Knudsen, B., Krizan, P., Lastovicka, J., Maeder, J., Orsolini, Y., Pyle, J. A., Rex, M., Vanicek, K., Weber, M., Wohltmann, I., Zanis, P., and Zerefos, C.: Ozone trends at northern mid- and high latitudes – a European perspective, Ann. Geophys., 26, 1207–1220, doi:10.5194/angeo-26-1207-2008, 2008.
Hegglin, M. I. and Shepherd, T. G.: Large climate-induced changes in ultraviolet index and stratosphere-to-troposphere ozone flux, Nature Geosci., 2, 687–691, doi:10.1038/ngeo604, 2009.
Hurrel, J.: Hurrel PC-Based North Atlantic Oscillation Index (Monthly), available online: http://www.cgd.ucar.edu/cas/jhurrell/indices.html, 2009.
Lait, L. R., Schoeberl, M. R., and Newman, P. A.: Quasi-Biennial modulation of the Antarctic ozone depletion, J. Geophys. Res.-Atmos., 94, 11559–11571, 1989.
Livezey, R. E. and Chen, W. Y.: Statistical field significance and its determination by Monte-Carlo techniques, Mon. Weather Rev., 111, 46–59, doi:10.1175/1520-0493(1983)111<0046:sfsaid>2.0.CO;2, 1983.
van Loon, H.: Half-yearly oscillations in middle and high southern latitudes and coreless winter, J. Atmos. Sci., 24, 472–486, 1967.
van Loon, H.: Half-yearly oscillations in Drake Passage, Deep-Sea Res., 19, 525–527 1972.

ACPD
12, 13161–13199, 2012

Mäder, J. A., Staehelin, J., Peter, T., Brunner, D., Rieder, H. E., and Stahel, W. A.: Evidence for the effectiveness of the Montreal Protocol to protect the ozone layer, Atmos. Chem. Phys., 10, 12161–12171, doi:10.5194/acp-10-12161-2010, 2010.
Müller, R., Grooß, J.-U., Lemmen, C., Heinze, D., Dameris, M., and Bodeker, G.: Simple measures of ozone depletion in the polar stratosphere, Atmos. Chem. Phys., 8, 251–264, doi:10.5194/acp-8-251-2008, 2008.
Naveau, P., Guillou, A., and Cooley, D.: Modelling pairwise dependence of maxima in space, Biometrika, 96, 1–17, 2009.
Newman, P. A., Daniel, J. S., Waugh, D. W., and Nash, E. R.: A new formulation of equivalent effective stratospheric chlorine (EESC), Atmos. Chem. Phys., 7, 4537–4552, doi:10.5194/acp-7-4537-2007, 2007.
Oltmans, S. J. and London, J.: The Quasi-Biennial Oscillation in atmospheric ozone, J. Geophys. Res.-Oc. Atmos., 87, 8981–8989, 1982.
Orsolini, Y. J. and Doblas-Reyes, F. J.: Ozone signatures of climate patterns over the Euro-Atlantic sector in the spring, Q. J. Roy. Meteorol. Soc., 129, 3251–3263, doi:10.1256/qj.02.165, 2003.
Orsolini, Y. J. and Limpasuvan, V.: The North Atlantic Oscillation and the occurrences of ozone miniholes, Geophys. Res. Lett., 28, 4099–4102, 2001.
Padoan, S., Ribatet, M., and Sisson, S.: Likelihood-based inference for max-stable processes, J. Am. Stat. Assoc., 105, 263–277, 2010.
Peter, T.: Microphysics and heterogeneous chemistry of polar stratospheric clouds, Annu. Rev. Phys. Chem., 48, 785–822, 1997.
Pickands, J.: Statistical inference using extreme order statistics, Ann. Stat., 3, 119–131, 1975.
Randel, W. J. and Cobb, J. B.: Coherent variations of monthly mean total ozone and lower stratospheric temperature, J. Geophys. Res.-Atmos., 99, 5433–5447, 1994.
Rex, M., Salawitch, R. J., von der Gathen, P., Harris, N. R. P., Chipperfield, M. P., and Naujokat, B.: Arctic ozone loss and climate change, Geophys. Res. Lett., 31, L04116, doi:10.1029/2003gl018844, 2004.
Ribatet, M., Cooley, D., and Davison, A. C.: Bayesian inference from composite likelihoods, with an application to spatial extremes, Stat. Sinica, 22, 813–845, 2012.
Rieder, H. E., Staehelin, J., Maeder, J. A., Peter, T., Ribatet, M., Davison, A. C., Stübi, R., Weihs, P., and Holawe, F.: Extreme events in total ozone over Arosa – Part 2: Fingerprints of

ACPD
12, 13161–13199, 2012

atmospheric dynamics and chemistry and effects on mean values and long-term changes, Atmos. Chem. Phys., 10, 10033–10045, doi:10.5194/acp-10-10033-2010, 2010a.
Rieder, H. E., Staehelin, J., Maeder, J. A., Peter, T., Ribatet, M., Davison, A. C., Stübi, R., Weihs, P., and Holawe, F.: Extreme events in total ozone over Arosa – Part 1: Application of extreme value theory, Atmos. Chem. Phys., 10, 10021–10031, doi:10.5194/acp-10-10021-2010, 2010b.
Rieder, H. E., Jancso, L. M., Di Rocco, S., Staehelin, J., Maeder, J. A., Peter, T., Ribatet, M., Davison, A. C., De Backer, H., Koehler, U., Krzyscin, J., and Vanicek, K.: Extreme events in total ozone over the northern mid-latitudes: an analysis based on long-term data sets from five European ground-based stations, Tellus B, 63, 860–874, doi:10.1111/j.1600-0889.2011.00575.x, 2011.
Rieder, H. E., Frossard, L., Ribatet, M., Staehelin, J., Maeder, J. A., Di Rocco, S., Davison, A. C., Peter, T., Weihs, P., and Holawe, F.: On the relationship between total ozone and atmospheric dynamics and chemistry at mid-latitudes – Part 2: The effects of the El Niño/Southern Oscillation, volcanic eruptions and contributions of atmospheric dynamics and chemistry to long-term total ozone changes, Atmos. Chem. Phys. Discuss., 12, 13201–13236, doi:10.5194/acpd-12-13201-2012, 2012.
Rue, H. and Held, L.: Gaussian Markov Random Fields: Theory and Applications, Monographs on Statistics and Applied Probability, Chapman and Hall, London, 104, 2005.
Sato, M., Hansen, J. E., McCormick, M. P., and Pollack, J. B.: Stratospheric aerosol optical depths, 1850–1990, J. Geophys. Res.-Atmos., 98, 22987–22994, 1993.
Schlather, M.: Models for stationary max-stable random fields, Extremes, 5, 33–44, 2002.
Schliep, E. M., Cooley, D., Sain, S. R., and Hoeting, J. A.: A comparison study of extreme precipitation from six different regional climate models via spatial hierarchical modeling, Extremes, 13, 219–239, doi:10.1007/s10687-009-0098-2, 2010.
Schnadt Poberaj, C., Staehelin, J., and Brunner, D.: Missing stratospheric ozone decrease at Southern Hemisphere middle latitudes after Mt. Pinatubo: a dynamical perspective, J. Atmos. Sci., 68, 1922–1945, 2011.
Shepherd, T. G.: Dynamics, stratospheric ozone, and climate change, Atmos.-Ocean, 46, 117–138, doi:10.3137/ao.460106, 2008.
Solomon, S.: Stratospheric ozone depletion: a review of concepts and history, Rev. Geophys., 37, 275–316, 1999.

ACPD
12, 13161–13199, 2012

SPARC CCMVal, SPARC Report on the Evaluation of Chemistry-Climate Models, edited by: Eyring, V., Shepherd, T. G., Waugh, D. W., SPARC Report No. 5, WCRP-132, WMO/TD-No. 1526, available at http://www.sparc-climate.org/publications/sparc-reports/, 2010.

Steinbrecht, W., Haßler, B., Brühl, C., Dameris, M., Giorgetta, M. A., Grewe, V., Manzini, E., Matthes, S., Schnadt, C., Steil, B., and Winkler, P.: Interannual variation patterns of total ozone and lower stratospheric temperature in observations and model simulations, Atmos. Chem. Phys., 6, 349–374, doi:10.5194/acp-6-349-2006, 2006.

Struthers, H., Bodeker, G. E., Austin, J., Bekki, S., Cionni, I., Dameris, M., Giorgetta, M. A., Grewe, V., Lefèvre, F., Lott, F., Manzini, E., Peter, T., Rozanov, E., and Schraner, M.: The simulation of the Antarctic ozone hole by chemistry-climate models, Atmos. Chem. Phys., 9, 6363–6376, doi:10.5194/acp-9-6363-2009, 2009.

Thompson, D. W. J. and Wallace, J. M.: Annular modes in the extratropical circulation. Part I: month-to-month variability, J. Climate, 13, 1000–1016, 2000.

Varin, C. and Vidoni, P.: A note on composite likelihood inference and model selection, Biometrika, 92, 519–528, 2005.

Ventura, V., Paciorek, C. J., and Risbey, J. S.: Controlling the proportion of falsely rejected hypotheses when conducting multiple tests with climatological data, J. Climate, 17, 4343–4356, doi:10.1175/3199.1, 2004.

Waugh, D. W. and Randel, W. J.: Climatology of arctic and antarctic polar vortices using elliptical diagnostics, J. Atmos. Sci., 56, 1594–1613, 1999.

Waugh, D. W., Oman, L., Kawa, S. R., Stolarski, R. S., Pawson, S., Douglass, A. R., Newman, P. A., and Nielsen, J. E.: Impacts of climate change on stratospheric ozone recovery, Geophys. Res. Lett., 36, L03805, doi:10.1029/2008gl036223, 2009.

WMO: Scientific Assessment of Ozone Depletion: 1994, World Meteorological Organization, Geneva, 1995.

WMO: Scientific Assessment of Ozone Depletion: 2002, Global Ozone Research and Montitoring Project, Geneva, 498, 2003.

WMO: Scientific Assessment of Ozone Depletion: 2006, Global Ozone Research and Montitoring Project, Geneva, 572, 2007.

WMO: Scientific Assessment of Ozone Depletion: 2010, Global Ozone Research and Montitoring Project, Geneva, 516, 2011.

ACPD
12, 13161–13199, 2012

Table 1. Overview of data sets used in this study. Data sets indicated with * are not available for the entire study period.

Data	Time range (resolution)	Source
Total Ozone	1979–2007 (daily)	Bodeker Scientific, NIWA 2.7 data set http://www.bodekerscientific.com/data/total-column-ozone
Solar Cycle	1979–2007 (monthly)	NOAA National Geophysical Data Center ftp://ftp.ngdc.noaa.gov/STP/SOLAR_DATA/SOLAR_RADIO/FLUX/Penticton_Adjusted/monthly/MONTHPLT.ADJ
QBO at 30 and 50 hPa	1979–2007 (monthly)	NOAA National Weather Service Climate Prediction Center http://www.cpc.noaa.gov/data/indices/
Nino 3.4 Index	1979–2007 (monthly)	NCAR/UCAR Climate and Global dynamics http://www.cgd.ucar.edu/cas/catalog/climind/TNI_N34/index.html
NAO Index	1979–2007 (monthly)	NCAR/UCAR Climate and Global dynamics http://climatedataguide.ucar.edu/guidance/hurrell-north-atlantic-oscillation-nao-index-pc-based
AAO Index	1979–2007 (monthly)	NOAA National Weather Service Climate Prediction Center http://www.cpc.noaa.gov/products/precip/CWlink/daily_ao_index/aao/monthly.aao.index.b79.current.ascii
SATO Index	1979–2000 (monthly)*	NASA Goddard Institute for Space studies http://data.giss.nasa.gov/modelforce/strataer/
ODS (in terms of EESC)	1979–2007 (monthly)	NASA Goddard Institute for Space studies http://acdb-ext.gsfc.nasa.gov/Data_services/automailer/

ACPD
12, 13161–13199, 2012

Table 2. Summary of the likelihood ratio tests between the annual (null hypothesis H_0) and seasonal (alternative hypothesis H_1) models for EHOs, ELOs and Mean Values (MV) at northern (NM) and southern (SM) mid-latitudes. The column CN indicates the number of grid cells out of 8640 for which H_0 is rejected at the 5 %-level and the column R gives the proportion of these grid cells (i.e., R = CN/8640).

Test level α = 5 %	CN	R
EHOs NM	8277	95.8 %
ELOs NM	8632	99.9 %
MV NM	5673	65.7 %
EHOs SM	7581	87.7 %
ELOs SM	8345	96.6 %
MV SM	4713	54.5 %

ACPD
12, 13161–13199, 2012

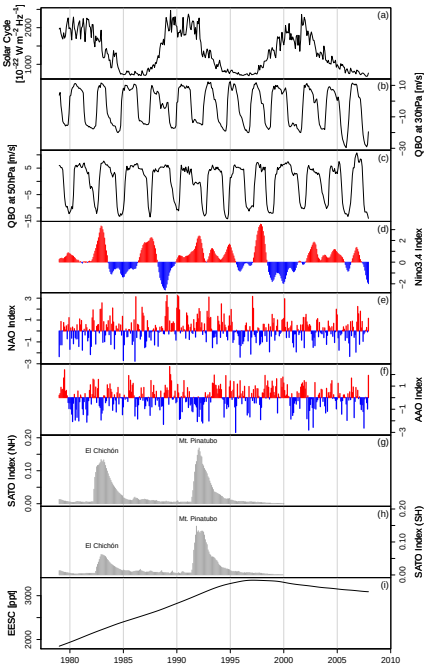

Fig. 1. Temporal evolution of the covariates used in this study: **(a)** solar cycle as light flux at 10.7 cm, **(b)** Quasi-Biennial Oscillation (QBO) Index at 30 hPa, **(c)** as **(b)** but at 50 hPa, **(d)** NINO 3.4 Index describing the state of the El Niño/Southern Oscillation (ENSO), **(e)** North Atlantic Oscillation (NAO) Index (principal components of the leading empirically-determined orthogonal function of sea level pressure anomalies over the Atlantic sector (20° N–80° N, 90° W–40° E) from Hurrel, 2009), **(f)** Antarctic Oscillation (AAO) Index, **(g)** volcanic aerosol loading in terms of mean optical thickness, SATO Index (Sato et al., 1993) for the Northern Hemisphere (major volcanic eruptions of El Chichón (1982) and Mt. Pinatubo (1991) are marked), **(h)** as **(g)** but for the Southern Hemisphere, and **(i)** atmospheric loading of ODS in terms of equivalent effective stratospheric chlorine (EESC). All covariates are given on a monthly basis. For information on the sources of the data sets for the individual covariates see Table 1.

ACPD
12, 13161–13199, 2012

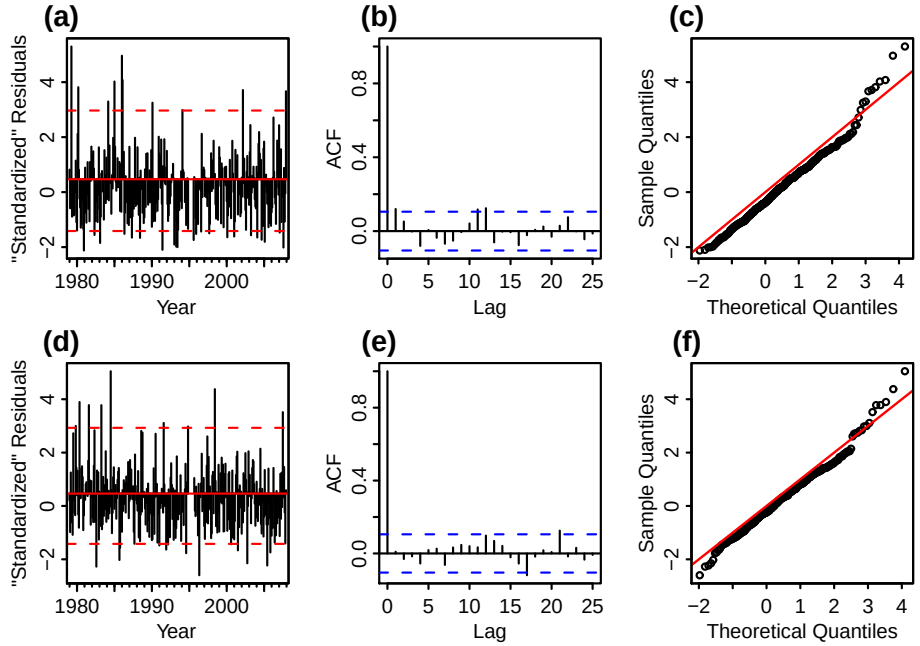

Fig. 2. Diagnostic plots of the extremes model with seasonal covariates for EHOs at two sample grid cells **(a)**–**(c)** 45.5° N, 93° W and **(d)**–**(f)** 45.5° S, 138° E. Panels **(a)** and **(d)** show "standardized" residuals $\left(y(t) - \mu(t)/\sigma\right)$ with 95 %-confidence bounds; panels **(b)** and **(e)** their correlograms and panels **(c)** and **(f)** the GEV(0,1,ξ) Q-Q plots with the identity line in red.

ACPD
12, 13161–13199, 2012

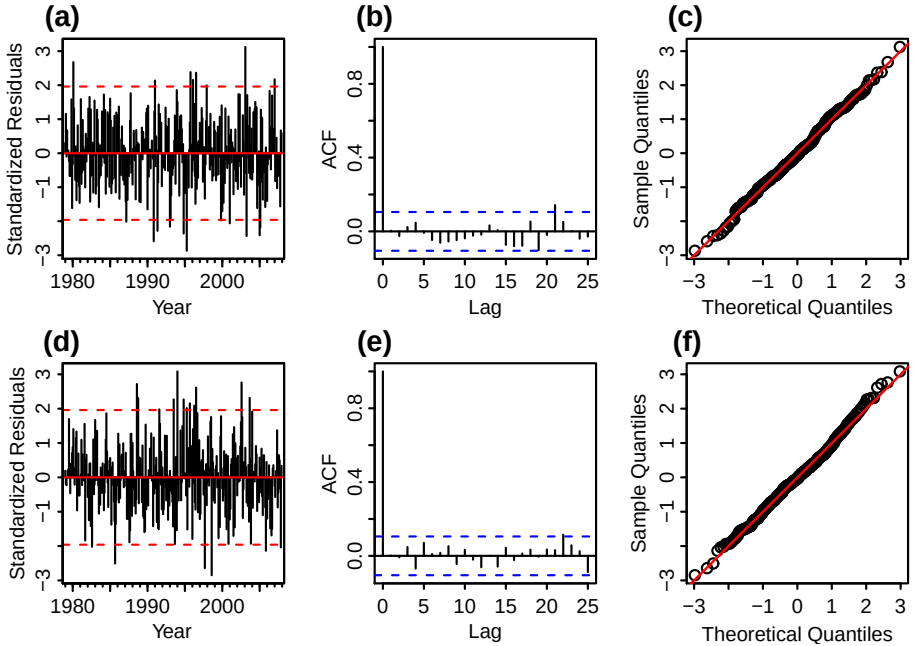

Fig. 3. Diagnostic plots of the ARMA(1,1) model with seasonal covariates for monthly mean values of column ozone at two sample grid cells **(a)**–**(c)** 45.5° N, 93° W and **(d)**–**(f)** 45.5° S, 138° E. Panels **(a)** and **(d)** show the standardized residuals with 95 %-confidence bounds; panels **(b)** and **(d)** their correlograms and panels **(c)** and **(f)** the normal Q-Q plots with the identity line in red.

ACPD
12, 13161–13199, 2012

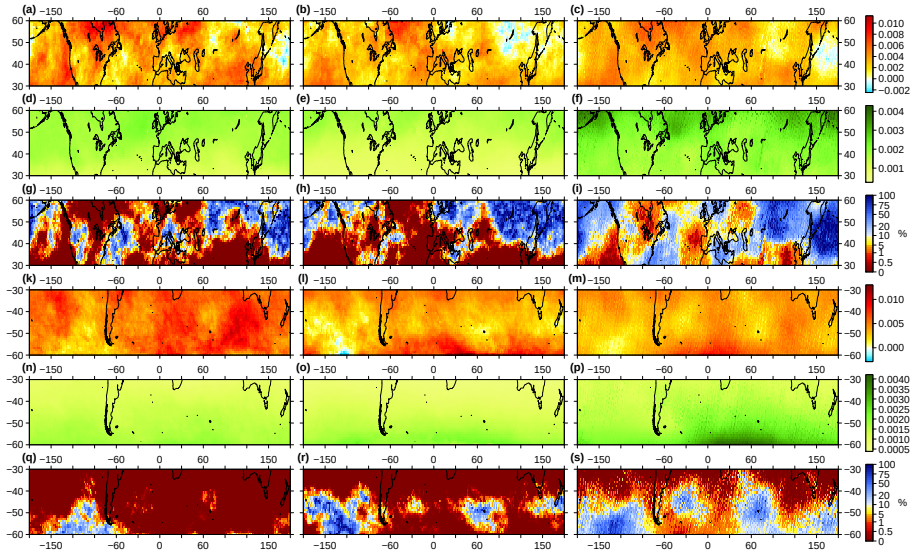

Fig. 4. Coefficient estimates (in DU 10^{22} W^{-1} m^2 Hz) for the solar cycle on an annual basis for **(a)** EHOs, **(b)** ELOs and **(c)** mean values at 30° N to 60° N; **(d)–(f)** show standard errors for the coefficients in **(a)–(c)** while **(g)–(i)** show the corresponding *p*-values. **(k)–(s)** as **(a)–(i)** but for 30° S to 60° S.

ACPD
12, 13161–13199, 2012

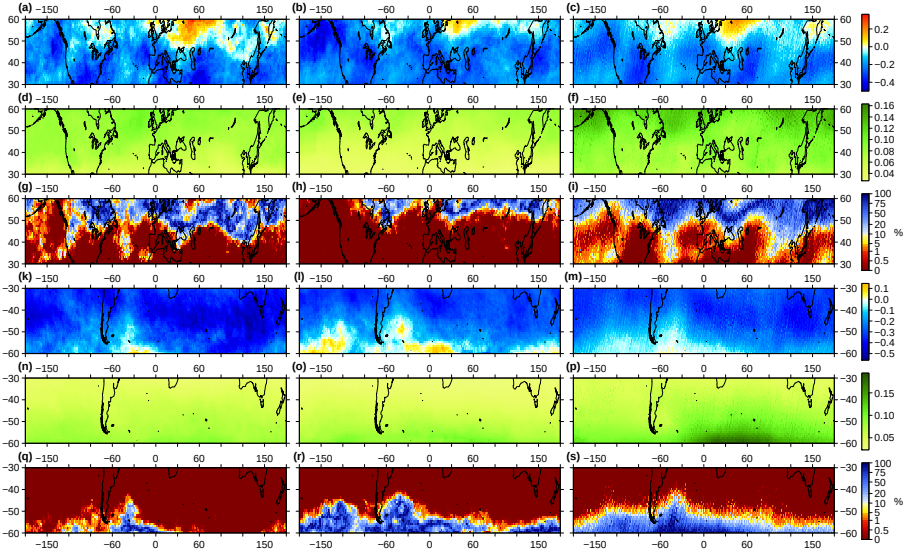

Fig. 5. Coefficient estimates (in $\mathrm{DU\,m^{-1}\,s}$) for the Quasi-Biennial Oscillation (at 30 hPa) on an annual basis for **(a)** EHOs, **(b)** ELOs and **(c)** mean values at 30° N to 60° N; **(d)–(f)** show standard errors for the coefficients in **(a)–(c)** while **(g)–(i)** show the corresponding *p*-values. **(k)–(s)** as **(a)–(i)** but for 30° S to 60° S.

ACPD
12, 13161–13199, 2012

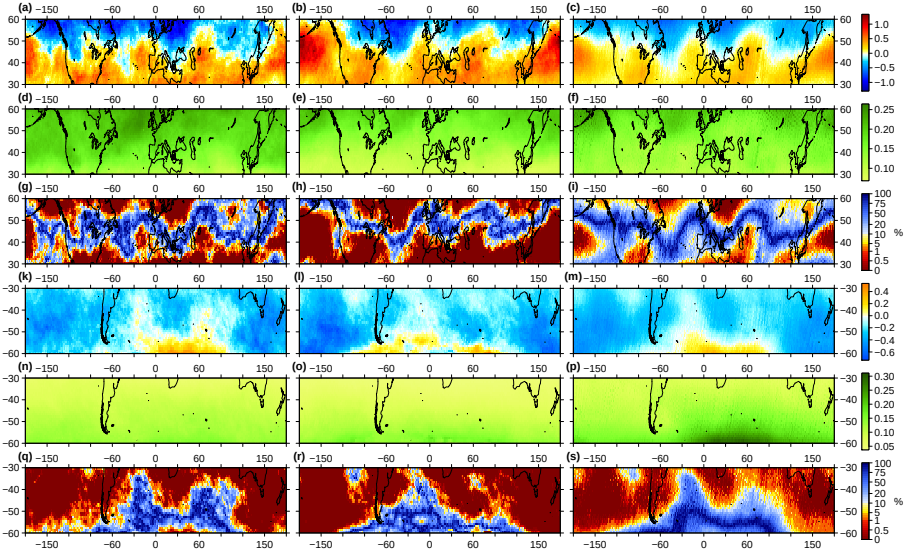

Fig. 6. Coefficient estimates (in DU m^{-1} s) for the Quasi-Biennial Oscillation (at 50 hPa) on an annual basis for **(a)** EHOs, **(b)** ELOs and **(c)** mean values at 30° N to 60° N; **(d)**–**(f)** show standard errors for the coefficients in **(a)**–**(c)** while **(g)**–**(i)** show the corresponding *p*-values. **(k)**–**(s)** as **(a)**–**(i)** but for 30° S to 60° S.

ACPD
12, 13161–13199, 2012

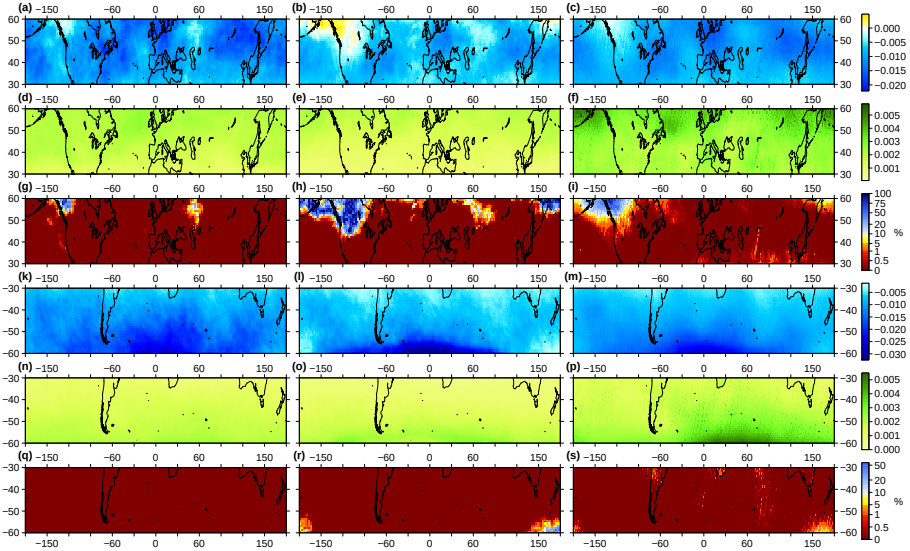

Fig. 7. Coefficient estimates (in DU ppt^{-1}) for ozone depleting substances in terms of equivalent effective stratospheric chlorine (EESC) on an annual basis for **(a)** EHOs, **(b)** ELOs and **(c)** mean values at 30° N to 60° N; **(d)**–**(f)** show standard errors for the coefficients in **(a)**–**(c)** while **(g)**–**(i)** show the corresponding *p*-values. **(k)**–**(s)** as **(a)**–**(i)** but for 30° S to 60° S.

ACPD
12, 13161–13199, 2012

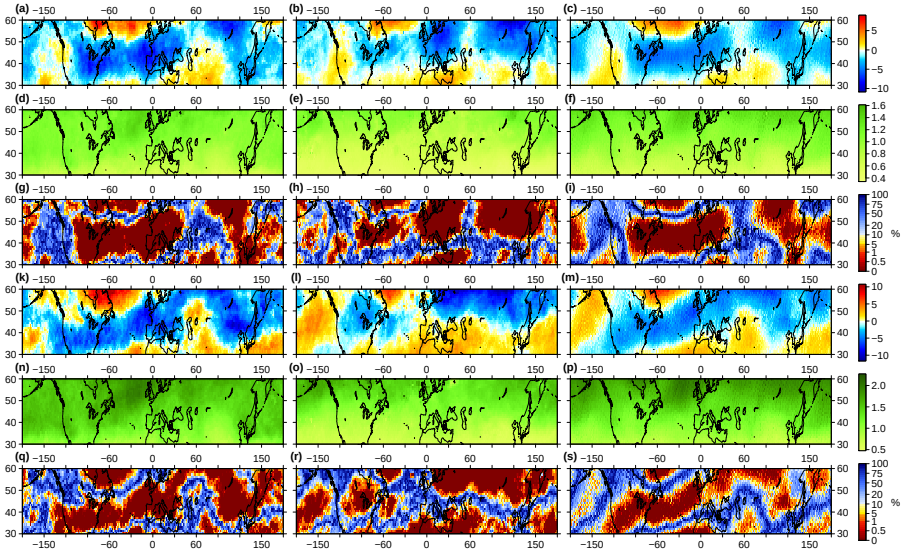

Fig. 8. Coefficient estimates (in DU (unit NAO)$^{-1}$) of the North Atlantic Oscillation (NAO) for **(a)** EHOs, **(b)** ELOs and **(c)** mean values of total ozone during winter (DJF) at 30° N to 60° N. **(d)**–**(f)** show corresponding standard errors for coefficients in **(a)**–**(c)** while **(g)**–**(i)** show *p*-values for coefficient estimates in **(a)**–**(c)**. **(k)**–**(s)** as **(a)**–**(i)** but for spring (MAM).

ACPD
12, 13161–13199, 2012

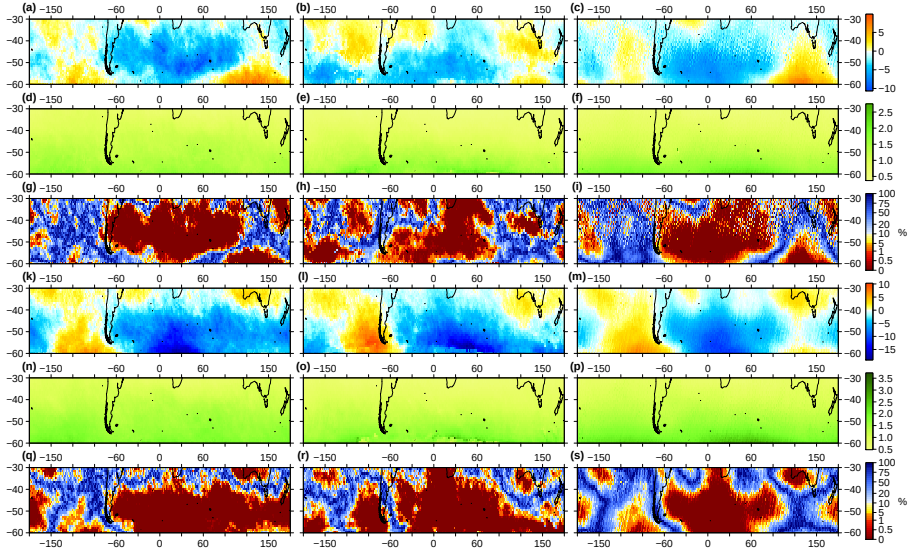

Fig. 9. Coefficient estimates (in DU (unit AAO)$^{-1}$) of the Antarctic Oscillation (AAO) for **(a)** EHOs, **(b)** ELOs and **(c)** mean values of total ozone during winter (JJA) at 30° S to 60° S. **(d)–(f)** show corresponding standard errors for coefficients in **(a)–(c)** while **(g)–(i)** show *p*-values for coefficient estimates in **(a)–(c)**. **(k)–(s)** as **(a)–(i)** but for spring (SON).

ACPD
12, 13161–13199, 2012